Li, Guozhu; Ning, Bai-Qi; Chu, Yen-Hsyang; Reid, Iain Murray; Dolman, Bronwyn Kaye
A comparison of lower thermospheric winds derived from range spread and specular meteor trail echoes Journal of Geophysical Research, 2012; 117:A03310.

http://hdl.handle.net/2440/72805

A comparison of lower thermospheric winds derived from range spread and specular meteor trail echoes

Guozhu Li,[1] Baiqi Ning,[1] Lianhuan Hu,[1] Yen-Hsyang Chu,[2] I. M. Reid,[3,4] and B. K. Dolman[3,4]

[1] Interferometry measurements of range spread meteor trail echoes (RSTEs; also known as nonspecular echoes) have provided new insights into both the irregularity structures in meteor trails and lower-thermospheric winds (LTWs). In this study, we used trail echoes observed with the newly installed Sanya (18.4°N, 109.6°E) 47.5 MHz VHF coherent radar and the Sanya all-sky meteor radar to estimate instantaneous zonal and hourly averaged meridional winds from RSTEs and hourly averaged zonal and meridional winds from large numbers of specular meteor echoes. The mean height variations in both the zonal and meridional winds estimated from the RSTEs were generally consistent with those estimated from specular meteor echoes below 96 km. This gives validity to the technique proposed recently by Oppenheim et al. (2009) and suggests that RSTE measurements made with a small radar can be used to investigate LTWs, whereas this had previously been limited to larger radars such as the Jicamarca radar. However, some observations show significant differences in wind magnitude at individual heights at times. The results of RSTE measurements show the presence of an intense westward wind with a speed near 100 ms^{-1}. In contrast, the specular meteor zonal winds were generally less than 50 ms^{-1}. On the other hand, the meridional drift of RSTEs derived from the meridional Doppler velocity at higher altitudes shows a very poor correlation with the specular meteor meridional wind. Potential causes for the discrepancy in wind estimates obtained from RSTE and specular meteor trail echoes are discussed.

1. Introduction

[2] The lower thermosphere (~90–120 km in altitude) has long been a region of interest for the atmospheric community investigating coupling between the lower and upper atmosphere. This region is not well understood owing to the difficulty of sounding, with the altitude too low for general scientific satellites and too high for balloons. Chemical release experiments made with sounding rockets can accurately measure wind profiles with high-altitude resolution in this region [e.g., *Larsen*, 2000, 2002; *Chu et al.*, 2007], but rocket-measured winds are typically infrequent in time, and sporadic in space. Optical instruments which detect airglow emissions from excited atoms or molecules have been employed to measure neutral winds in the lower-thermosphere region [*Rees et al.*, 1990], but are generally limited to specific altitudes, such as the O_1 557.7 nm emission from about 97 km, the O_2 865 nm emission from around 92 km, the Na 589.3 nm from around 90 km, and the OH 982 nm emission from around 86 km.

[3] Ground-based radars operating in the MF to VHF bands have been proven to be an effective method to monitor background winds, waves and tides in the lower-thermosphere region, where electron density irregularities serve as the targets responsible for the radar returns [e.g., *Vincent and Reid*, 1983; *Kudeki et al.*, 1993; *Holdsworth et al.*, 2004; *Fritts et al.*, 2010, and references therein]. On the basis of the Doppler frequency shift of specular meteor trail echoes detected by HF and VHF radars, the neutral wind velocity in the mesosphere and lower-thermosphere (MLT) region (about 80–100 km) is estimated. The temporal and spatial averaging typically used for the wind measurements is typically 1 h and 2 km, respectively. In addition to the use of the full correlation analysis (FCA) technique to measure horizontal wind velocities from 80 to 100 km, using partial reflection echoes from weakly ionized irregularities, MF radars have the potential to detect meteor echoes for wind measurement with a height resolution of about 2 km [*Tsutsumi et al.*, 1999; *Hall et al.*, 2004]. In general, the mean wind speeds retrieved from specular meteor trail echoes are less than 100 ms^{-1}, which is in contrast to

[1]Beijing National Observatory of Space Environment, Institute of Geology and Geophysics, Chinese Academy of Sciences, Beijing, China.
[2]Institute of Space Science, National Central University, Chung-Li, Taiwan.
[3]Department of Physics and Mathematical Physics, University of Adelaide, Adelaide, South Australia, Australia.
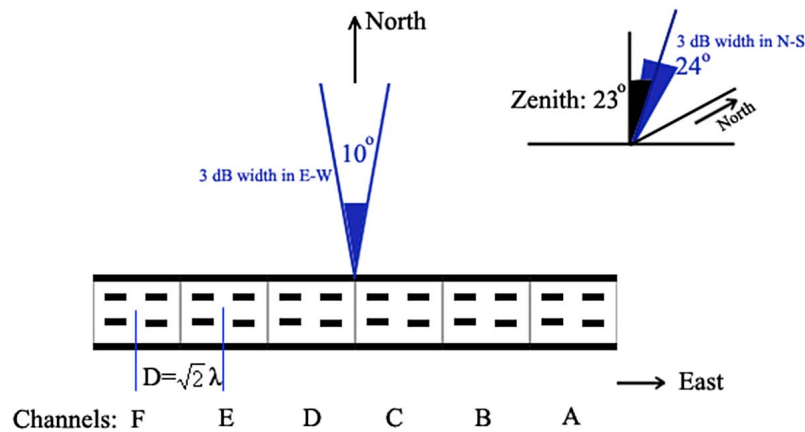[4]ATRAD Pty Ltd., Adelaide, South Australia, Australia.

Figure 1. Schematic of the antenna array (12 × 2 Yagi antennas with six modules) for coherent backscatter radar. All modules were used for transmission and reception with a beam axis zenith angle of 23°. The easternmost and westernmost modules (A and F) were used for interferometry analysis to derive the zonal drifts of 3-m-scale irregularities.

instantaneous wind speeds which can be as large as 150 ms^{-1} or more, as measured using chemical release experiments in the MLT region [e.g., *Chu et al.*, 2007; *Larsen and Fesen*, 2009]. *Larsen* [2000] reported the extraordinarily large winds are not an uncommon feature in the MLT region. It has been suggested the large winds are associated with vertically propagating inertiogravity waves with large amplitudes [*Chu et al.*, 2007]. Considering the measured wind differences, comparisons between these different techniques is useful for increasing our understanding and making better use of the respective measurements. Earlier comparisons, including the studies by *Grime et al.* [2000], *Franke et al.* [2001], and *Liu et al.* [2002], show general agreement in the wind patterns extracted from different instruments, but also show significant differences in the instantaneous wind profiles at individual times. *Larsen et al.* [2003] performed a comparison of lidar and sounding rocket chemical tracer wind measurements, and found excellent agreement both in the magnitude and the vertical structure in the profiles.

[4] Specular meteor trail echoes generally appear in one range bin, last approximately 1 s, and can be used to derive the neutral wind. A second type of long-lived meteor trail echo, which appears in successive range bins, with lifetimes ranging from a few seconds to several minutes, can also be used to measure background winds [*Oppenheim et al.*, 2009]. Such echoes are known as range spread trail echoes (RSTE, or nonspecular meteor trail echoes) and are believed to result from Bragg scattering from field-aligned irregularities generated in the meteor trail through Farley-Buneman or gradient drift (FBGD) instabilities [e.g., *Oppenheim and Dimant*, 2006; *Dyrud et al.*, 2007; *Oppenheim et al.*, 2008; *Sugar et al.*, 2010]. By treating RSTE as the tracers of neutral winds, *Oppenheim et al.* [2009] developed a new method of measuring wind velocity profiles. These authors suggested that a radar with an aperture smaller than the Jicamarca Radio Observatory high-power, large-aperture (JRO-HPLA) radar used in their study could be utilized to make similar measurements, provided it had an interferometric capability, and could steer a radar beam in the direction perpendicular to the geomagnetic field line. Wind estimates obtained from RSTEs differ from estimates made

from specular meteor trail echoes, as the former provides short-term wind profiles and the latter gives a long-term average result [*Chapin and Kudeki*, 1994].

[5] The objective of the present work is to investigate simultaneous wind measurements from RSTEs and specular meteor trail echoes. The newly installed 47.5 MHz VHF coherent backscatter radar, and all-sky meteor radar that are colocated at Sanya (18.4°N, 109.6°E) in Hainan Island, China, provide an opportunity to validate the wind measurement technique developed by *Oppenheim et al.* [2009], using a small radar, instead of a large ISR (e.g., the Jicamarca radar) for the first time. These two radars were operated alternately during experimental periods to detect RSTEs using the coherent backscatter radar, and specular meteor echoes using the all-sky meteor radar. The neutral winds derived from RSTEs and numerous specular echoes are presented and compared. The results show that patterns of wind profiles are generally consistent between instruments, but large discrepancies in the wind magnitudes are frequently observed at individual heights. Possible factors responsible for the differences, including the background electric field, RSTE aspect sensitivity and measurement differences are discussed.

2. Experimental Details

[6] The two VHF radars were operated at a nominal frequency of 47.5 MHz, with a peak power of 24 kW. The meteor trail experiments were conducted in a successive sequence of 1 min for coherent backscatter echoes and 1 min for specular meteor echoes. As a result, a total of 30 min of data were recorded for each mode during a 1 h observation period. In the following, the characteristics of the coherent backscatter radar and all-sky meteor radar are briefly introduced.

2.1. Coherent Backscatter Radar

[7] This radar was operated to detect echoes scatted from *E*-region field-aligned irregularities. As shown in Figure 1, the antenna array consists of 24 (12 × 2) five-element Yagi antennas, arranged in a linear configuration with the long axis aligned in the east-west direction. The array comprises
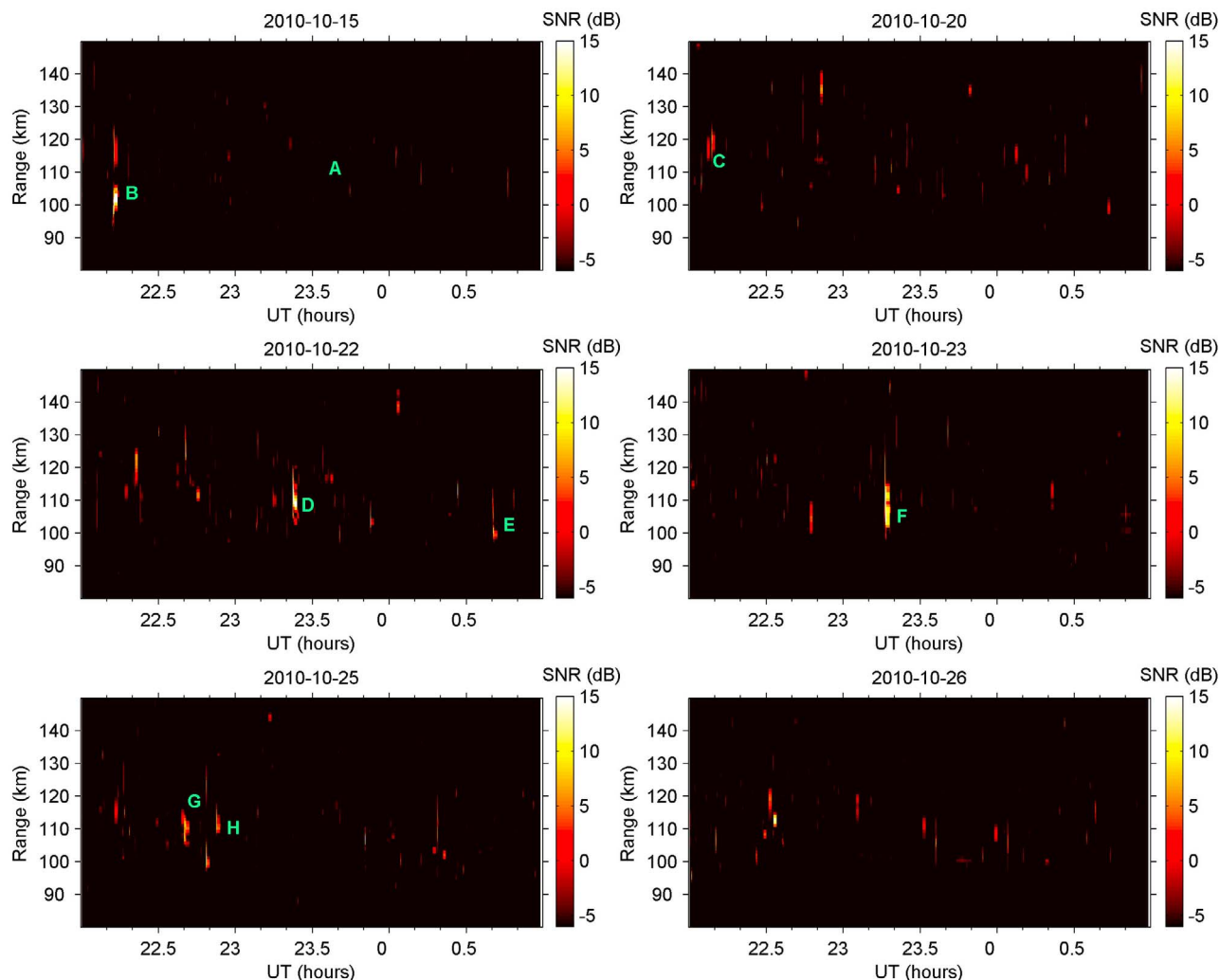
Figure 2. Range-time-intensity (RTI) maps of meteor-induced backscatter echoes. The short-lived and long-duration range spread trail echo (RSTE) cases are marked as A and B–H, respectively.

six identical modules that can detect echoes separately and independently. The separation between adjacent modules is $\sqrt{2}\lambda$, where λ specifies the radar wavelength. The antenna beam of the whole array is in a fanlike shape with 3 dB beam width 10° in the azimuth and 24° in the elevation directions. The main antenna beam was pointed toward north at a zenith angle of 23°, such that it is perpendicular to the local magnetic field in the E region. The pulse repetition frequency (PRF) was 650 Hz and the radar pulse length was 6 μs. This corresponds to a range resolution of 0.9 km within the sampled range interval of 80–200.6 km. A 256-point FFT algorithm was used to compute the Doppler spectra of the radar returns, with a Doppler velocity window of ± 257 ms^{-1} and a resolution of 2 ms^{-1}. Received complex signals at every range gate were coherently integrated 4 times, and stored in a time series with a length of 8930 points (1 min) for later offline interferometry analysis.

2.2. All-Sky Meteor Radar

[8] The interferometric radar was used to detect the returns reflected from specular meteor trails. A PRF of 430 Hz and a height range from 70 to 110 km were used for meteor trail

detection. The antenna array consists of one crossed dipole antenna for transmission, and five crossed dipole antennas for reception. The mean winds are determined by fitting a mean horizontal wind in each 2 km altitude bin to each half-hourly or hourly averaged radial velocity derived from the specular meteor trails. Detailed descriptions of the meteor detection technique and subsequent estimation of the wind profile can be found in the work of *Holdsworth et al.* [2004].

3. Observational Results

[9] Figure 2 shows the range-time-intensity (RTI) plots of radar echoes observed by the Sanya VHF coherent scatter radar in the morning hours 2200–0100 UT (0530–0830 LT) on 15, 20, 22–23, and 25–26 October 2010. Inspection of Figure 2 indicates that during these there are no E-region field-aligned irregularity (FAI) echoes that arise from scattering from the background ionization layer. The lighter streaks represent the radar returns from the meteor trails, which often cover several range bins and occur mainly between 95 and 130 km. The slant range of 95–130 km corresponds to heights of about 87–120 km when the beam
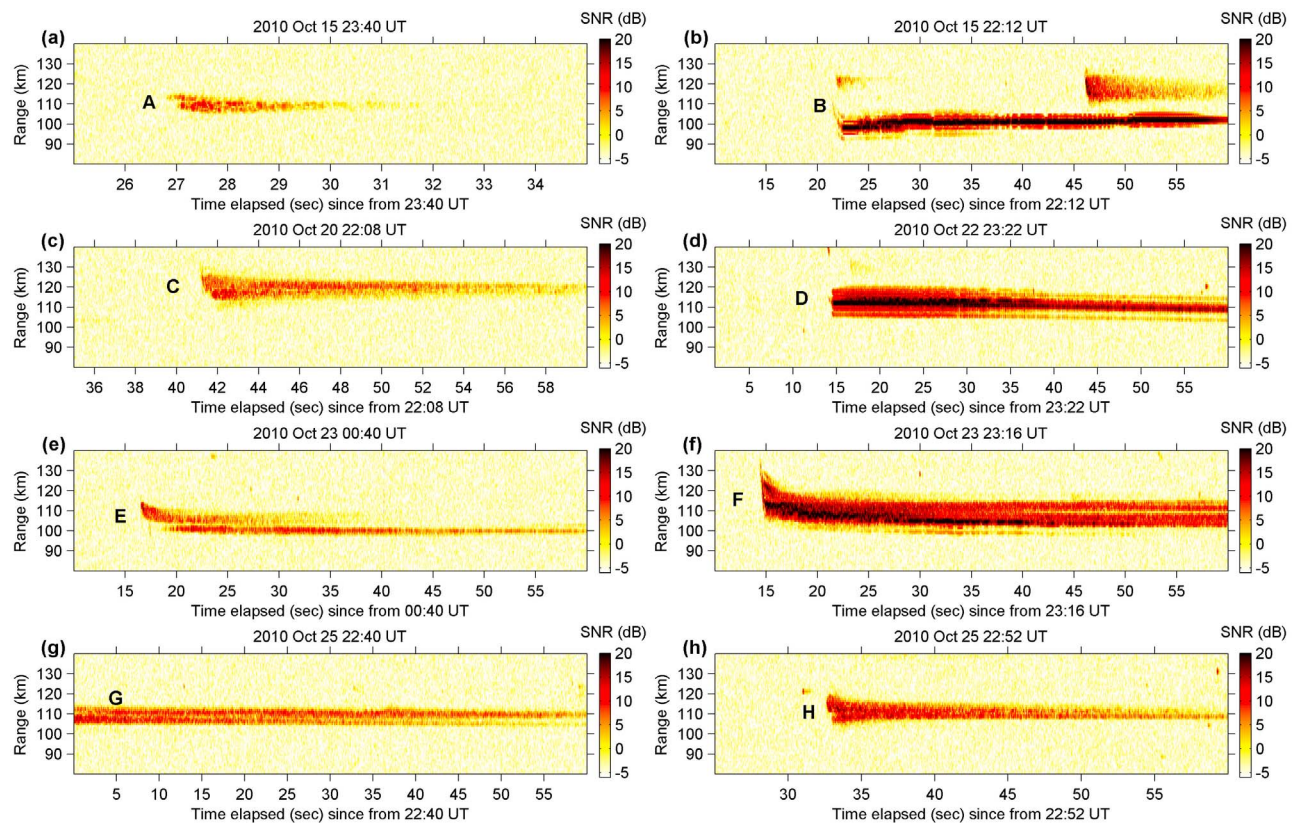
Figure 3. RTI maps of the selected short-lived and long-duration RSTE cases A–H. Note that the horizontal scale is second.

is perpendicular to the magnetic field (**B**). This RSTE height distribution is similar to that reported by *Sugar et al.* [2010]. The lifetimes of most trail echoes are less than 5 s (see, e.g., case A shown in Figure 2). During the morning hours, such short-lived RSTE events are often observed, with a typical occurrence rate of about 10 echoes h^{-1} within the slant range of 100–110 km. In addition to these short-lived trails, there are a number of meteor trail echoes which persist for more than 15 s with signal-to-noise ratios (SNR) greater than 10 dB. *Malhotra et al.* [2007] defined long-duration echoes to be echoes lasting more than 15 s. Since the short-lived echoes are not suitable for interferometric analysis and wind profile determination due to the low-radar PRF, in the following analysis we will only use the long-duration RSTE cases to derive the zonal wind. Such cases have been marked as B–H in Figure 2. For short-lived RSTEs, the Doppler velocities will be utilized to estimate the hourly averaged meridional wind.

3.1. Range Spread Trail Echo (RSTE) Cases

[10] Figure 3 shows the RTI plots of selected RSTE cases, including one short-lived RSTE, event A, observed on 15 October and seven long-duration RSTE cases, events B–H, observed on 15, 20, 22–23, and 25 October 2010, respectively. As seen in Figure 3a, the short-lived event A was observed near 110 km in slant range, lasting for about 3 s, with a SNR > 5 dB. Utilizing numerical model simulations with a wavelength of 6.4 m and a dip angle of 51°, *Zhou et al.* [2004] investigated the aspect sensitivity of RSTEs, and

found that although the maximum power from RSTEs will be detected when the radar is pointed perpendicular to **B**, substantial power can still be obtained in the off-perpendicular direction. *Close et al.* [2008] examined the cutoff angle for RSTE detection by steering the ALTAIR beam away from perpendicular to **B** in small increments. Those authors found the aspect sensitivity cutoff angle lies around 78°, and more than 90% of echoes were scattered from the region with an angle ≥85°. They found that the radar sensitivity to range spread trails falls off at approximately 3 ± 2 dB per degree, as the radar points progressively away from the region perpendicular to **B**. In the following analysis of hourly averaged meridional drifts of RSTEs, the selected echoes were required to have a SNR > 5 dB, and a duration >2 s, in order to reduce the effects of echoes scattered from a direction too far from the region perpendicular to **B**. Figures 3b–3h show the RTI images of the long-duration RSTE events. It is clearly seen in Figures 3b, 3d, and 3f, that the echo strength is stronger than the other cases. Such strong echoes indicate the scattering was most likely from the trails of especially large meteoroid events. We also note that in Figure 3g, due to the alternative observations of RSTEs and specular meteor echoes, the onset of meteor trails was not detected by the VHF coherent scatter radar.

[11] The range variations of the self-normalized Doppler spectra of the short- and long- duration RSTE events A, B, F, and G are presented in Figures 4a–4d, respectively. For the short-lived RSTE case shown in Figure 4a, the spectra in every range bin within 106–111 km contain a large low-frequency peak, and many narrow higher-frequency peaks.
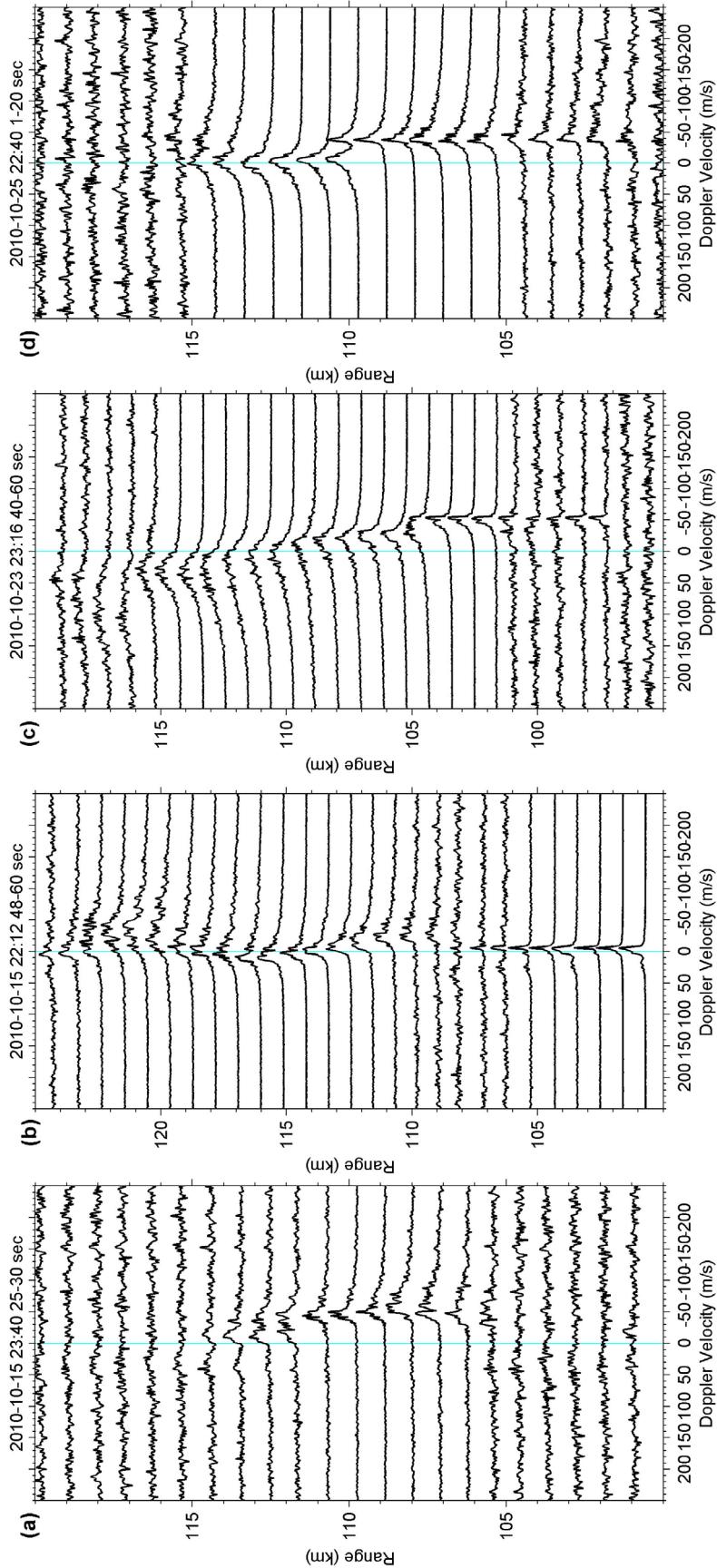
Figure 4. Range variations of Doppler spectra at selected times for the short-lived and long-duration RSTE cases A, B, F, and G.

The latter appeared mainly on the spectral side corresponding to a negative Doppler velocity (i.e., toward the radar). These high-frequency asymmetric wings of the spectra are similar to those of range spread meteor trail echoes detected by the Jicamarca coherent VHF radar. It is clear from Figure 4b that the Doppler spectra below 106 km are consistent. A similar feature can also be noted in Figure 4c. For meteor trail irregularities, the nearly invariant Doppler velocities with altitude are not uncommon features. For example, using the Chungli VHF radar observations, *Chu and Wang* [2003] observed similarity in the Doppler spectra of RSTEs below 143 km (in range). On the other hand, for the case presented in Figure 4d, two notable features are seen. The first is that the spectra in range bins above 110 km are nearly symmetric. This feature seems to suggest that the high-frequency plasma waves in the meteor trails were excited initially, and then decayed with time, leaving nearly symmetric spectra after about 15 s [*Chapin and Kudeki*, 1994]. Second, a surprising feature of the observed trail echoes is that in the upper- and lower-range bins, the Doppler velocities show pronounced differences, with respective values near 0 ms^{-1} and 40 ms^{-1}. Such a feature may be associated with the mechanism of structured vertical wind shear [e.g., *Chu and Wang*, 2003; *Bourdillon et al.*, 2005]. We shall not pursue this issue any further in the present work since the central objective is to investigate simultaneous wind measurements from RSTEs and specular meteor trail echoes. In fact, a negative vertical shear with westward wind above and eastward wind below was observed for the RSTE and specular meteor wind measurements at that time. This will be investigated in the following section in detail.

3.2. Comparison of Zonal Winds Derived From RSTEs and Specular Echoes

[12] To determine the zonal drift velocity of the long-duration meteor trails, the phase differences between the easternmost and westernmost channels were calculated using the interferometry technique described by *Farley et al.* [1981] and *Oppenheim et al.* [2009]. A 64-point complex FFT was used to compute the raw amplitude autospectra of the meteor trail echoes for each channel. By multiplying a pair of the raw amplitude autospectra, and then dividing the averaged result by the square root of the product of the raw power autospectra with a 10 times average, the normalized cross spectra of the two channel signals, written as

$$S_{WE}(\omega) = \frac{\left\langle V_W(\omega) V_E^*(\omega) \right\rangle}{\left\langle |V_W(\omega)|^2 \right\rangle^{1/2} \left\langle |V_E(\omega)|^2 \right\rangle^{\frac{1}{2}}},$$

were calculated (for additional details, see *Farley et al.* [1981]). From the complex normalized cross spectrum, S_{WE}, we obtained the coherence value (magnitude, $|S_{WE}|$) and phase difference between the two channel signals during a time interval of 4.2 s.

[13] Figures 5a–5c show examples of the interferometry results for the long-duration RSTE cases F and G, during different time intervals, for range bins 107 km, 110.6 km and 106.1 km, respectively. In each set, the top panels show the amplitude (coherency) of the cross spectrum, and the bottom panels show the phase difference in degrees. The phase differences with coherence values of more than 0.9 are shown as red dots. An increase in phase difference (from negative to positive) corresponds to a displacement of the echoing region to the west. As seen in Figure 5a, the spectral amplitude is generally larger than 0.8, and the phase difference is close to a constant value at a fixed time interval. During these intervals, the phase differences with coherence values >0.9 exhibit an apparent ascending trend, that is, there is a clear westward drift at 107 km for the meteor trail irregularities observed at 2316 UT. For the RSTE case G presented in Figures 5b and 5c, we note that although the scattered values of phase differences cover a wide extent of phase angle, the phase differences with coherence values >0.9 are confined at a narrow range, and can be clearly identified. Furthermore, as seen from Figures 5b and 5c, the trail irregularities observed at 2240 UT exhibit opposite drift, toward the west and east at range bins of 110.6 and 106.1 km, respectively. For the present interferometry analysis, a phase difference ($\delta\varphi$) of 5° at 100 km altitude (h) corresponds to the displacement of 196.3 m according to $\delta x = h\delta\varphi/kd$, where k is $2\pi/\lambda$. Therefore, the time rate of the phase difference provides an estimation of the apparent zonal drift velocity. More phase differences and estimated zonal drift velocities for the RSTE cases F and G are shown in Figure 6. Note that the vertical scale shown in Figures 6b and 6d is height, estimated using $R \cos 23°$, where R is range. Considering that the meteor trail echo could be scattered from an off-perpendicular direction, our height estimates could be biased. However, as mentioned earlier, the trail signal strength falls off as 3 dB per degree as the radar beam is steered away from perpendicular to **B**. If the number 3 dB applies for our measurements, the long-duration RSTEs with SNR > 10 dB should be scattered from the region with an angle greater than 85°. This implies that for a range of 100 km, biases in the height estimates are less than 4 km.

[14] As shown in Figure 6a, the blue dots (sometimes shown as blue bold lines because the values get very close to each other) represent the phase differences. The mean phase difference (φ) at a fixed time is shown as a red dot and shifted rightward 2.1 s for clarity. By computing the difference ($\delta\varphi$) of the mean value φ between two adjacent intervals according to the above formula, we can estimate the drift velocity ν_n. For a single long-duration RSTE event, there will be some values of ν_n ($n = 1$–13) at a fixed altitude. We discarded the maximum and minimum values of ν_n, and then took the mean value of ν_n as the zonal drift velocity. For comparison we also fitted the slope of the phase differences between channels and estimated the drift velocity following the procedure of *Oppenheim et al.* [2009]. Figure 6b shows the velocity profile derived from the RSTE case F, observed at 2326 UT, 23 October 2010. The horizontal error bars show the standard deviations. The velocities marked with red asterisks (96–101 km) result from the phase differences shown in Figure 6a. It is clear from Figures 6a and 6b that the rapid changes in phase angle occurred (marked as black solid lines) when the trail irregularities moved through the antenna beam, and induced the large standard errors of drift velocities at 96 and 96.8 km, whereas the irregularities generally drifted westward within the height range of 94–105 km. Figures 6c and 6d show the velocity measurements of another RSTE case G observed at
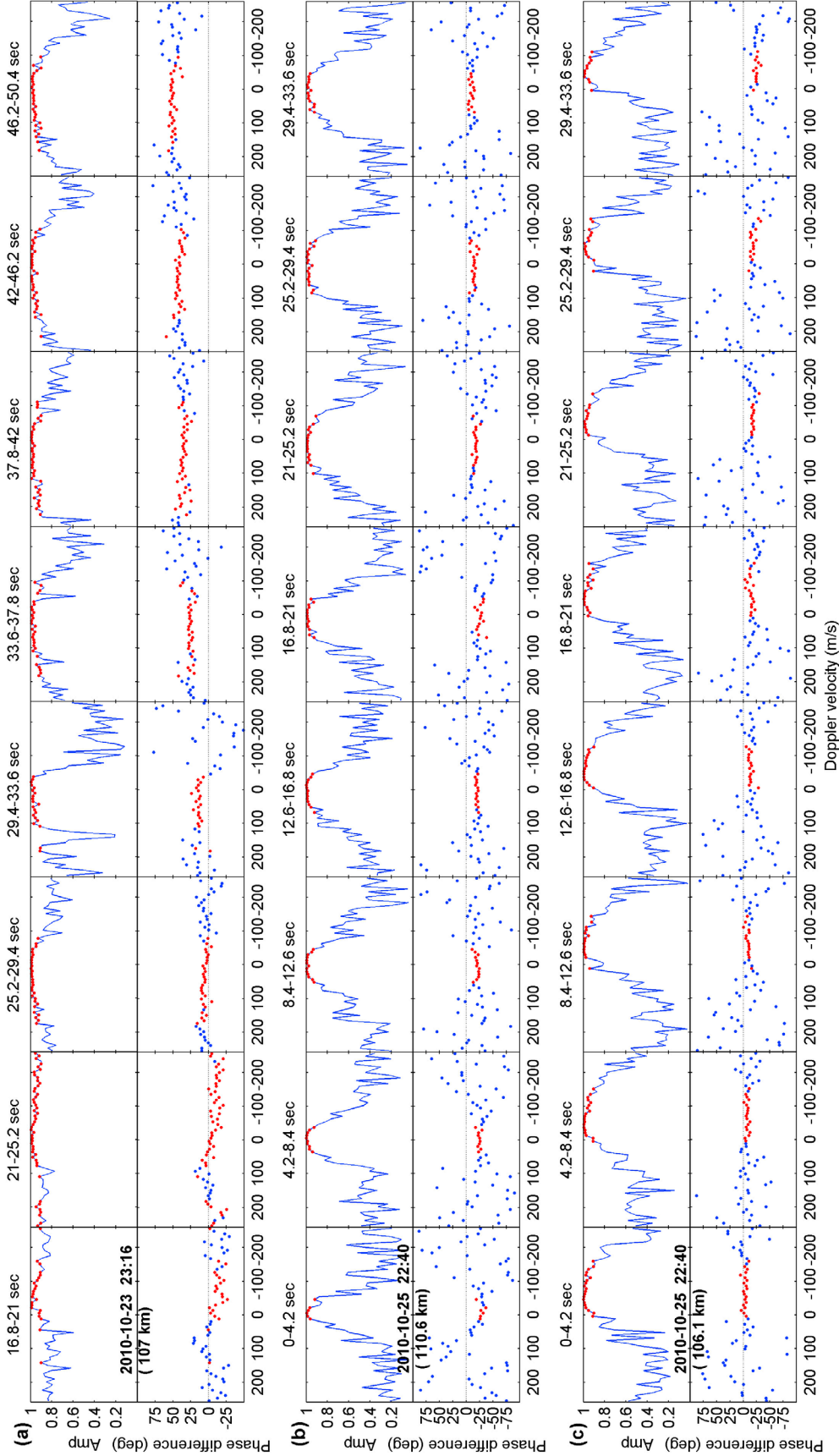
Figure 5. Examples of the interferometry results for the long-duration RSTE cases observed on 23 and 25 October 2010. (top) Magnitudes of normalized cross spectra. (bottom) Phase angles. The red dots represent the values with coherency >0.9. An increase in phase difference from negative to positive indicates a westward drift.
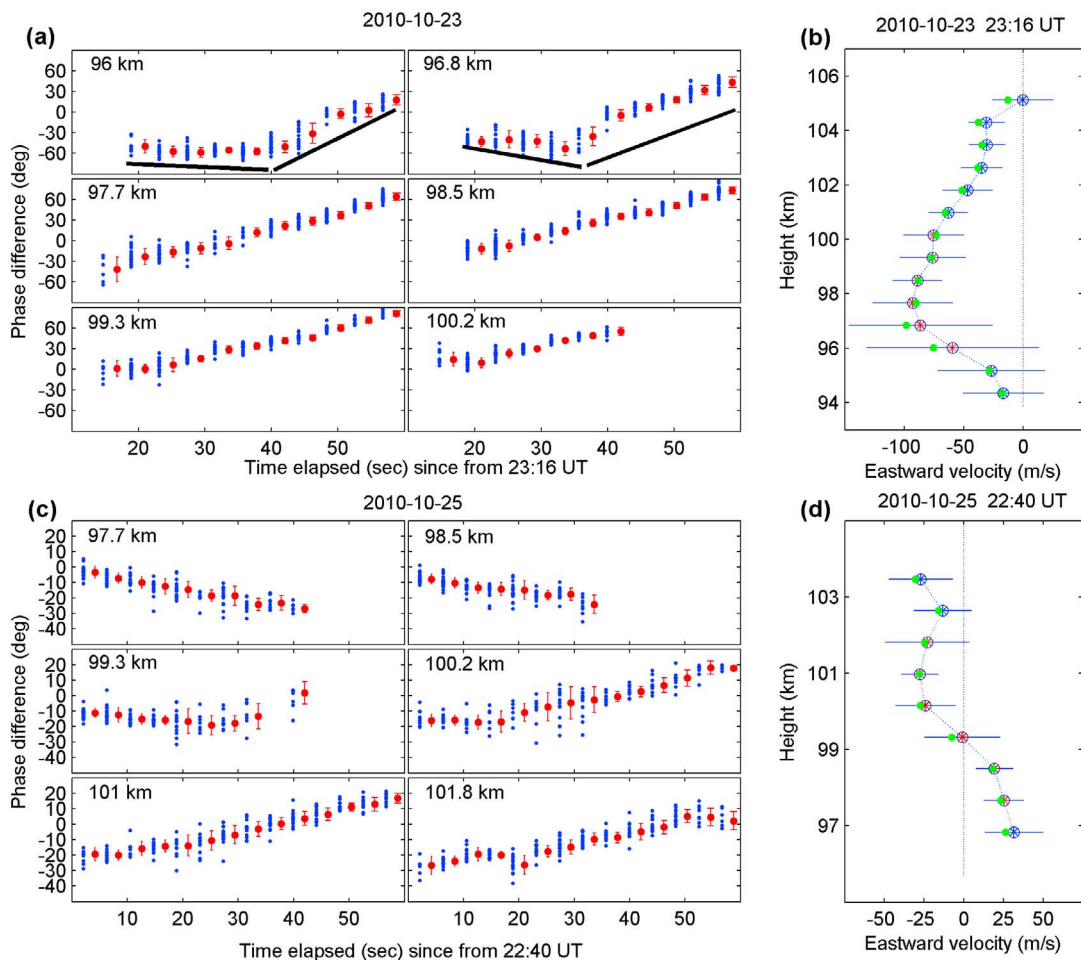
Figure 6. (a, c) The phase angles derived from interferometric analysis of RSTE cases F (23 October) and G (25 October). The red dots show the mean values of phase angles at a fixed time interval, which is shifted rightward 2.1 s. (b, d) Zonal velocities derived from the variations of phase angles. The velocities shown as red asterisks in Figures 6b and 6d correspond to the variations of phase angles shown in Figures 6a and 6c, respectively. The velocities shown as green dots in Figures 6b and 6d are estimated following the procedure of *Oppenheim et al.* [2009].

2240 UT, 25 October 2010. It can be inferred that the zonal drift has an obvious shear from 25 ms^{-1} to -25 ms^{-1}, with westward winds above and eastward winds below. Furthermore, it is evident from Figures 6b and 6d that the zonal velocities estimated by the two methods (marked as blue circles and green dots) are generally similar. For other long-duration RSTE cases presented in Figure 2, the phase differences in the format of Figures 5 and 6 will not be shown here.

[15] Using the simultaneous wind observations derived from specular meteor echoes using the all-sky meteor radar, we performed a comparison of zonal winds obtained from both techniques. The hourly and half-hourly averaged wind speed (red and green lines) estimated from specular meteor echoes, and the instantaneous wind profiles estimated from single RSTE events are shown in Figure 7. Since the height resolution of specular meteor wind estimates is 2 km, a three-point running mean in altitude is performed over RSTE wind observations. It is clear from Figure 7a that this RSTE event occurred above 100 km. From Figure 2 we note that there are still several other high-altitude long-duration

RSTE cases. However, because the number of specular meteors detected above 100 km is usually not large enough for the estimation of wind velocities, such high-altitude RSTE cases will not be used for comparison here. Figure 7b shows the half-hourly averaged specular winds and instantaneous RSTE winds are both westward above 94 km. An increase in the westward wind is seen at altitudes of 94–98 km. However, the magnitude of instantaneous RSTE winds is definitely larger than that of half-hourly averaged specular winds. The discrepancy becomes more evident in the height range near 96–99 km, where the variations in the hourly mean wind and half-hourly mean wind show opposite trends. A similar wind pattern is also seen in Figure 7e, where the specular winds and RSTE wind are both eastward. Figure 7c shows a comparison of two RSTE wind profiles with specular meteor winds. It is clear that both the patterns of the wind profile, and the magnitude of the wind velocities, varied significantly over short time intervals at some heights. The wind velocities measured at 2240 UT in the 98–100 km range changed from approximately 25 ms^{-1} eastward to 25 ms^{-1} westward, indicating an apparent wind shear with a
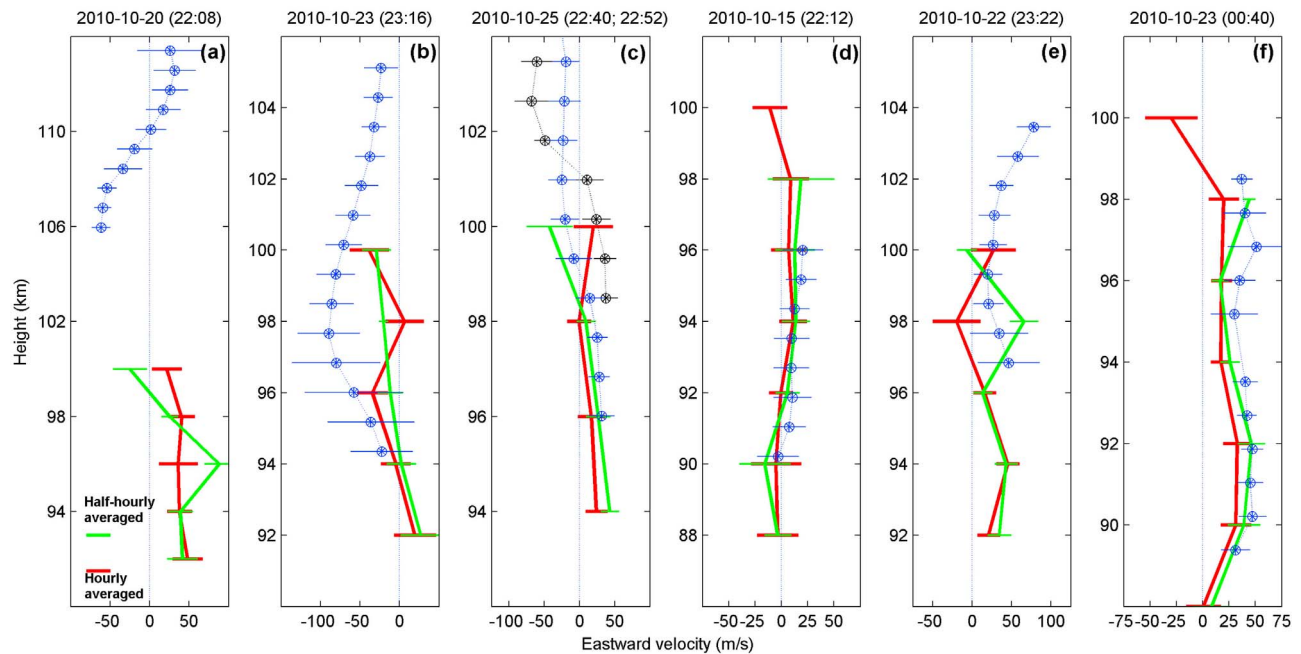
Figure 7. Comparisons of instantaneous zonal wind profiles derived from long-duration RSTEs (circle-dotted line), half-hourly (green line), and hourly (red line) averaged wind profiles from specular meteor echoes. A three-point running mean in altitude is performed over RSTE wind observations. Blue and black circles in Figure 7c show the velocity profiles derived from the RSTEs observed at 2240 UT and 2252 UT, respectively.

magnitude of 25 ms^{-1} km^{-1}. The shear magnitude is comparable to the half-hourly averaged specular meteor wind. However, just 12 min later, at 2252 UT, the RSTE wind velocity profile indicates the wind shear node has ascended to an altitude of 100–102 km. Given the magnetic aspect sensitivity of RSTEs (with several degrees for modest signal strength), the height difference (2 km) between the two shear nodes could be induced by the height estimation using R cos 23°. The comparisons presented in Figures 7d and 7f show good agreement in both the overall trends and in the magnitudes of the two sets of wind measurements. It is also clear from Figures 7d and 7f that the differences between hourly and half-hourly averaged specular meteor winds are very small.

3.3. Comparison of Meridional Winds Derived From RSTEs and Specular Echoes

[16] The Sanya VHF coherent backscatter radar antenna array is aligned east-west, so the RSTE meridional drift cannot be derived from interferometry analysis. However, the Doppler velocity observed by coherent radar is the phase velocity of the plasma waves. Therefore, we can estimate the meridional drifts of RSTEs from the Doppler velocity measurements. Actually, in many studies, the Doppler velocities have been used to extract meridional neutral winds from the backscatter data below 100 km altitude [e.g., *Murthy et al.*, 1998; *Patra et al.*, 2007]. Since the Sanya VHF coherent radar points northward with a zenith angle of 23° (perpendicular to the magnetic field in the E region), and with the assumptions that the zonal influences are negligible and the vertical wind is zero, the meridional drifts (v) of

RSTEs have been derived from the Doppler velocities (V_d) using the expression $v = V_d/\sin\theta$.

[17] Figure 8 shows the meridional winds in the height region 80–100 km, derived from RSTEs and specular meteor echoes. As seen in Figure 8a, the meridional velocities estimated from RSTEs have been suitably averaged to obtain a height resolution of 2 km, and time resolution of 1 h, similar to that of the meridional winds from specular meteor echoes, and shown as red and black lines, representing northward and southward drifts, respectively. When the number of RSTEs within a 2 km height interval during a 1 h period is less than 3, the associated RSTE drift values are not used. The green (blue) lines show the northward (southward) meridional specular meteor winds. To further distinguish them, RSTE meridional winds have been plotted at a shift of 0.4 km downward in the y axis. It is clear that the RSTE meridional velocities show similar behavior with specular meteor winds. In general, the higher- (lower-) altitude velocities obtained from both RSTEs and specular meteor echoes are southward (northward). The wind amplitudes also correspond well; for example, the velocities observed above 92 km at 2330 UT (22 October), and below 90 km at 2230 UT (15 October) and 0030 UT (21 October). In order to see the statistical behavior of their agreement, the meridional velocities are plotted as scatterplots in Figures 8b and 8c, for height regions 80–94 km, and 96–100 km, respectively. The standard deviations of RSTE mean meridional velocities are superimposed on the scatterplots. It can be seen that the correlation coefficient and slope are 0.82 and 0.63 for lower altitudes, indicating a strong correlation between the mean meridional RSTE and specular meteor
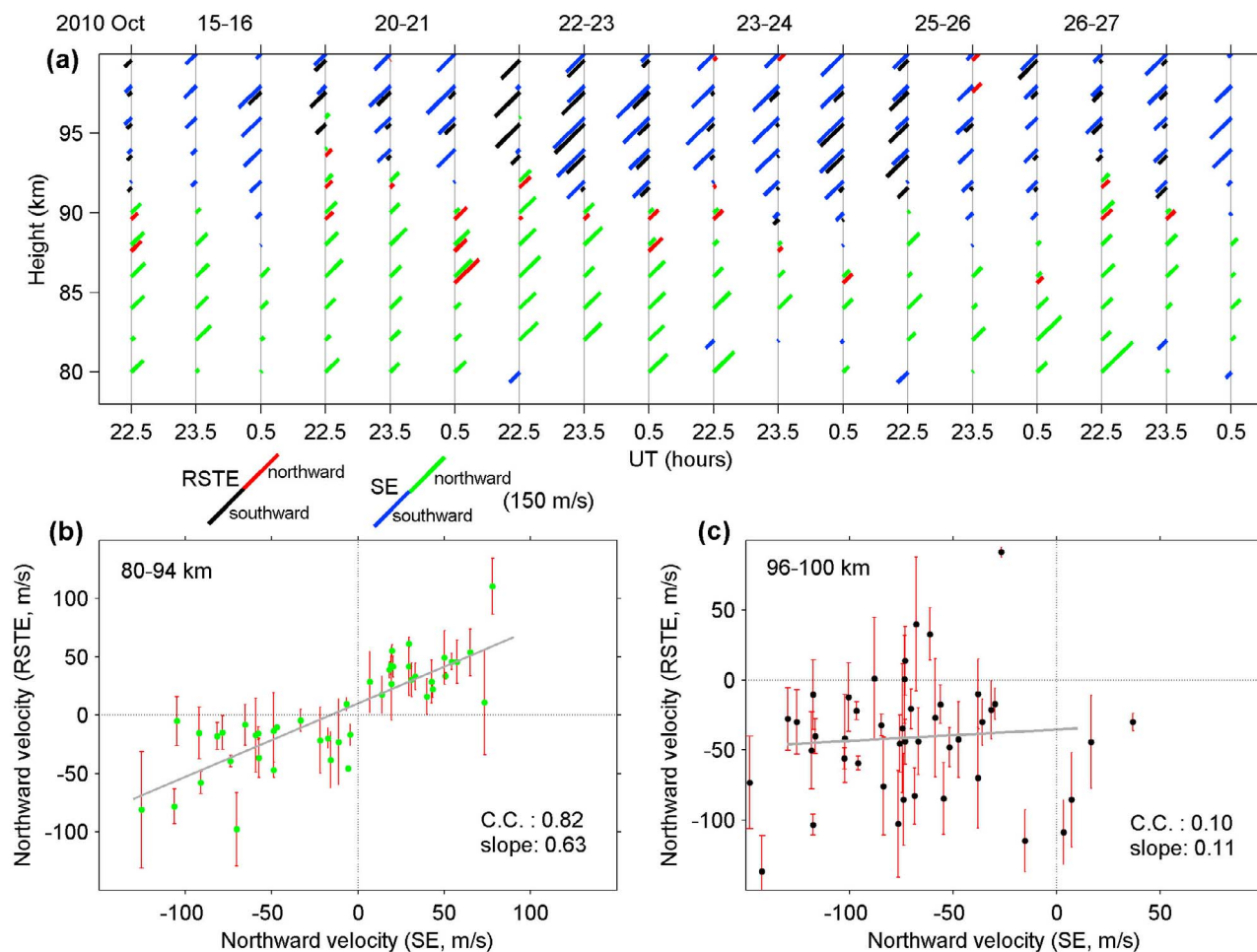
Figure 8. (a) A comparison of hourly averaged meridional RSTE drift (red and black lines) and specular meteor wind (green and blue lines). RSTE velocities are plotted at a shift of 0.4 km downward. (b, c) Scatterplots and least squares fits for the RSTE meridional drifts and specular meteor meridional winds within an altitude range 80–94 km and 96–100 km. Correlation coefficient and slope are also shown.

winds below 94 km. For higher altitudes, the correlation coefficient and slope are only 0.1 and 0.11, respectively.

4. Discussion

[18] In general, the comparison of neutral winds obtained from RSTEs and specular meteor trail echoes shows good agreement between their patterns below 96 km. Using numerous RSTEs obtained from JRO-HPLA radar, *Oppenheim et al.* [2009] examined RSTE wind profiles and found that the measured wind profiles were consistent with each other. However, they did not compare their results to an independent technique. The present study of simultaneous wind measurements from RSTEs and specular meteor trail echoes not only gives validity to the techniques proposed by *Oppenheim et al.* [2009], but also confirms that the RSTE observations from the small Sanya coherent backscatter radar can be utilized to estimate wind profiles.

[19] In addition, the observations also present some differences between the magnitudes of RSTE and specular meteor zonal winds for individual heights at times. There are four potential reasons for the observed difference in the zonal wind estimations. The first is that in our experiment,

only the zonal baseline antenna array is used, and so the RSTE zonal wind could be biased by the meridional motions of the trails since it is not possible to uniquely determine the meteor trail locations. The comparisons between the incoherent scatter radar and the coherent scatter radar measurements have shown that the scattering angles are less restrictive, and that extended horizontal layers can produce scattering over a broad radar range [e.g., *Hysell et al.*, 2004, and references therein]. The changes in the interferometric phase angles produced by horizontal meridional motion could also be interpreted as being associated with zonal motion. By considering meteor trails drift with a speed of 50 ms^{-1} at different positions throughout the sky for different drift directions, *Chapin and Kudeki* [1994] reported that at Jicamarca, the bias effect on velocity estimates is less than 10%, due to the low zenith angle of Jicamarca VHF radar. For the Sanya VHF radar, the zenith angle is 23°, and the errors in the zonal velocity estimates could be up to 20%, depending on the trail orientation [*Chapin and Kudeki*, 1994, Figure 14]. As seen in Figure 7, the maximum magnitude of RSTE winds is around 100 ms^{-1}. Thus the biases in the RSTE wind estimates are less than 20 ms^{-1}. *Chapin and Kudeki* [1994] suggested the trend with larger zenith

angle can underestimate the magnitude of the zonal drift velocity. If so, the obviously larger RSTE wind than specular meteor wind shown in Figure 7b cannot be ascribed to the effect of meridional motions of meteor trails.

[20] The second consideration is the ambient electric field effect. This can result in situations where meteor trail motions may not accurately reflect atmospheric wind speeds during the very early stages of trail evolution. However, at later times, a trail which breaks into pieces due to turbulence will more accurately track the neutral winds [e.g., *Oppenheim et al.*, 2000]. On the other hand, the RSTEs have been used to estimate neutral winds at Jicamarca (dip 1°), which is located in the *EEJ* region. Since the RSTE wind measurements work well at Jicamarca, the RSTEs observed at Sanya can also be used to estimate neutral wind since Sanya (dip 13°) is situated off the *EEJ* region. Further, in the present cases (shown in Figure 2), no *Es* associated irregularity echoes were detected. This may indicate that the ambient electric field (in the vertical direction) is weak. In such conditions, it seems likely that the large differences in the zonal wind shown in Figure 7 are not induced by the ambient electric field. It is also worth mentioning that if the electric field contributes to the zonal wind difference, magnitude of the difference between both winds could be large at higher altitude and small at lower altitude. Such a feature is not seen in Figure 7. The third is that the probing volumes of the two radars are different. It is to be remembered that the meteor radar estimates winds from numerous specular meteor trail echoes, which distributed randomly over a horizontal region with a diameter of several hundred kilometers. The coherent radar uses a narrow beam, and hence estimates winds from RSTEs from a narrow spatial range only. As such, small-scale horizontal wind perturbations may not be observed by the meteor radar due to the spatial average effect, but can be detected by the coherent radar. Finally, the differences in zonal winds estimated from RSTEs and specular meteor echoes could be ascribed to the fact that the RSTE measurements are instantaneous and therefore the winds are more susceptible to fast atmospheric perturbations. As seen in Figure 6a, the phase differences obviously display two different slopes at a single altitude (96 and 96.8 km) within a time interval of about 1 min. Such a change of slope most likely indicates there are substantial atmospheric perturbations creating temporal and spatial variations in the wind. Earlier studies have shown that the spatial and temporal fluctuations in the wind field associated with gravity waves tend to increase with altitude, especially above 96 km [*Gardner et al.*, 2002]. Furthermore, the winds measured by the all-sky meteor radar are averaged over a period greater than 30 min, and hence the specular meteor winds tend to have smaller variability in altitude. In fact, referring to Figure 7, we note that when the difference between half-hourly and hourly averaged specular winds is small, the discrepancy between RSTE and specular meteor winds also becomes small; for example the lower-altitude winds shown in Figures 7b and 7c, and the overall profiles shown in Figures 7d and 7f. On the other hand, Figure 7 shows that the hourly and half-hourly averaged specular winds differ substantially. In such conditions, it is quite possible that the zonal wind differences between the two techniques result from the long time averaged effect of the specular meteor wind.

[21] The comparison of the mean meridional RSTE wind and specular meteor wind generally shows good agreement below 96 km. As seen in Figure 8b, the statistical analysis shows that at lower altitudes, the correlation coefficient is 0.8. At higher altitudes, the comparison becomes more complicated, but the wind direction is mostly similar. This is consistent with the fact that the collisional effects are predominant, and the Doppler velocities are governed mainly by neutral winds in the lower-altitude region [e.g., *Chau et al.*, 2002]. Thus the meridional drift velocity (*v*) of RSTE can be approximately estimated from the simple expression $v = V_d/\sin\theta$. At altitudes above 96 km, the $\mathbf{E} \times \mathbf{B}$ drifts start to dominate, where $\mathbf{E}$ represents zonal electric field. As seen from Figure 8c, we note that the derived RSTE meridional winds show opposite directions with specular meteor winds at times, for example on 23 and 25 October. This could be caused by the enhanced zonal electric field effects on meridional Doppler velocity measurements at higher altitudes. Another possible cause of the difference is due to nonzero vertical winds. While the vertical velocities are significant, the meridional bias associated with vertical drift may not be removed by the average of 4 (or more) RSTE measurements within 1 h. An examination of specular meteor vertical wind shows that the maximum vertical wind is only 15 ms^{-1} during the observation periods, indicating biases induced by the vertical drifts in the RSTE horizontal wind estimates are very small.

5. Summary

[22] Using the Sanya VHF radar observations carried out during the morning hours of several days in October 2010 using coherent backscatter and specular meteor modes alternately, we compared the lower-thermospheric winds obtained from RSTEs and specular meteor trail echoes. In general, the height profiles of neutral winds derived from both RSTEs and specular meteor trail echoes show similar patterns. The results validate the technique proposed by *Oppenheim et al.* [2009] and provide a high degree of confidence in measurements of lower-thermospheric winds estimated from RSTEs with the Sanya coherent backscatter radar. However, RSTE zonal winds show much larger velocities than the specular meteor trail winds at some altitudes, where the peak RSTE wind velocity has been estimated to be up to about 100 ms^{-1}. Considering the obvious magnitude differences between half-hourly and hourly averaged specular meteor winds at times, we suggest the corresponding discrepancy in magnitude between RSTE instantaneous and specular meteor zonal wind profiles is most likely the result of the relatively long time averages required in the determination of the wind from specular meteor echoes.

[23] Furthermore, the meridional drift of RSTEs derived from Doppler velocities shows good agreement with the meridional meteor wind in the lower *E* region below 96 km with a correlation coefficient of 0.8. This high correlation coefficient in the lower-altitude region indicates that the mean wind derived from RSTE Doppler velocities could represent the meridional neutral wind and so be utilized to investigate tidal and planetary waves. In the near future, we will expand the Sanya VHF coherent backscatter radar array by installing two sub antenna arrays aligned in the north-

south direction. Using this updated configuration, RSTE positions can then be determined uniquely, reducing the height uncertainties in the zonal wind estimates.

References

Bourdillon, A., C. Haldoupis, C. Hanuise, Y. Le Roux, and J. Menard (2005), Long duration meteor echoes characterized by Doppler spectrum bifurcation, *Geophys. Res. Lett.*, 32, L05805, doi:10.1029/2004GL021685.

Chapin, E., and E. Kudeki (1994), Radar interferometric imaging studies of long-duration meteor echoes observed at Jicamarca, *J. Geophys. Res.*, 99, 8937–8949, doi:10.1029/93JA03198.

Chau, J. L., R. F. Woodman, and L. A. Flores (2002), Statistical character-istics of low-latitude ionospheric field-aligned irregularities obtained with the Piura VHF radar, *Ann. Geophys.*, 20, 1203–1212, doi:10.5194/angeo-20-1203-2002.

Chu, Y. H., and C. Y. Wang (2003), Interferometry observations of VHF backscatter from plasma irregularities induced by meteor in sporadic E region, *Geophys. Res. Lett.*, 30(24), 2239, doi:10.1029/2003GL017703.

Chu, Y. H., C. L. Su, M. F. Larsen, and C. K. Chao (2007), First measure-ments of neutral wind and turbulence in the mesosphere and lower ther-mosphere over Taiwan with a chemical release experiment, *J. Geophys. Res.*, 112, A02301, doi:10.1029/2005JA011560.

Close, S., T. Hamlin, M. Oppenheim, L. Cox, and P. Colestock (2008), Dependence of radar signal strength on frequency and aspect angle of nonspecular meteor trails, *J. Geophys. Res.*, 113, A06203, doi:10.1029/2007JA012647.

Dyrud, L. P., E. Kudeki, and M. M. Oppenheim (2007), Modeling long duration meteor trails, *J. Geophys. Res.*, 112, A12307, doi:10.1029/2007JA012692.

Farley, D., H. Ierkic, and B. Fejer (1981), Radar interferometry: A new technique for studying plasma turbulence in the ionosphere, *J. Geophys. Res.*, 86, 1467–1472, doi:10.1029/JA086iA03p01467.

Franke, S. J., E. Stoll, R. J. States, and C. S. Gardnerv (2001), Comparison of Na Doppler lidar and MF radar measurements of meridional winds in the mesosphere above Urbana, IL, *J. Atmos. Sol. Terr. Phys.*, 63, 1789–1796.

Fritts, D. C., et al. (2010), Southern Argentina Agile Meteor Radar: System design and initial measurements of large-scale winds and tides, *J. Geophys. Res.*, 115, D18112, doi:10.1029/2010JD013850.

Gardner, C. S., Y. Zhao, and A. Z. Liu (2002), Atmospheric stability and gravity wave dissipation in the mesopause region, *J. Atmos. Sol. Terr. Phys.*, 64, 923–929, doi:10.1016/S1364-6826(02)00047-0.

Grime, B. W., T. J. Kane, A. Z. Liu, G. Papen, C. S. Gardner, M. C. Kelley, C. Kruschwitz, and J. Drummond (2000), Meteor trail advection observed during the 1998 Leonid shower, *Geophys. Res. Lett.*, 27, 1819–1822, doi:10.1029/1999GL003699.

Hall, C. M., T. Aso, M. Tsutsumi, J. Höffner, and F. Sigernes (2004), Multi-instrument derivation of 90 km temperatures over Svalbard (78°N 16°E), *Radio Sci.*, 39, RS6001, doi:10.1029/2004RS003069.

Holdsworth, D. A., I. M. Reid, and M. A. Cervera (2004), Buckland Park all-sky interferometric meteor radar, *Radio Sci.*, 39, RS5009, doi:10.1029/2003RS003014.

Hysell, D. L., M. F. Larsen, and Q. H. Zhou (2004), Common volume coherent and incoherent scatter radar observations of mid-latitude sporadic E-layers and QP echoes, *Ann. Geophys.*, 22, 3277–3290.

Kudeki, E., P. K. Rastogi, and F. Sürücü (1993), Systematic errors in radar wind estimation: Implications for comparative measurements, *Radio Sci.*, 28, 169–179, doi:10.1029/92RS01931.

Larsen, M. F. (2000), Coqui 2: Mesospheric and lower thermospheric wind observations over Puerto Rico, *Geophys. Res. Lett.*, 27, 445–448, doi:10.1029/1999GL010704.

Larsen, M. F. (2002), Winds and shears in the mesosphere and lower ther-mosphere: Results from four decades of chemical release wind measure-ments, *J. Geophys. Res.*, 107(A8), 1215, doi:10.1029/2001JA000218.

Larsen, M. F., and C. G. Fesen (2009), Accuracy issues of the existing ther-mospheric wind models: Can we rely on them in seeking solutions to wind-driven problems?, *Ann. Geophys.*, 27, 2277–2284, doi:10.5194/angeo-27-2277-2009.

Larsen, M. F., A. Z. Liu, R. L. Bishop, and J. H. Hecht (2003), TOMEX: A comparison of lidar and sounding rocket chemical tracer wind measure-ments, *Geophys. Res. Lett.*, 30(7), 1375, doi:10.1029/2002GL015678.

Liu, A. Z., W. K. Hocking, S. J. Franke, and T. Thayaparan (2002), Com-parison of Na lidar and meteor wind measurements at Starfire Optical Range, NM, USA, *J. Atmos. Sol. Terr. Phys.*, 64, 31–40, doi:10.1016/S1364-6826(01)00095-5.

Malhotra, A., J. D. Mathews, and J. Urbina (2007), A radio science perspec-tive on long-duration meteor trails, *J. Geophys. Res.*, 112, A12303, doi:10.1029/2007JA012576.

Murthy, B. V. K., S. Ravindran, K. S. Viswanathan, K. S. V. Subbarao, A. K. Patra, and P. B. Rao (1998), Small-scale ($\sim$3 m) E region irregularities at and off the magnetic equator, *J. Geophys. Res.*, 103, 20,761–20,773, doi:10.1029/98JA00928.

Oppenheim, M. M., and Y. Dimant (2006), Meteor induced ridge and trough formation and the structuring of the nighttime E-region iono-sphere, *Geophys. Res. Lett.*, 33, L24105, doi:10.1029/2006GL028267.

Oppenheim, M. M., A. F. vom Endt, and L. P. Dyrud (2000), Electrody-namics of meteor trail evolution in the equatorial E-region ionosphere, *Geophys. Res. Lett.*, 27, 3173–3176, doi:10.1029/1999GL000013.

Oppenheim, M. M., G. Sugar, E. Bass, Y. S. Dimant, and J. Chau (2008), Day to night variation in meteor trail measurements: Evidence for a new theory of plasma trail evolution, *Geophys. Res. Lett.*, 35, L03102, doi:10.1029/2007GL032347.

Oppenheim, M. M., G. Sugar, N. O. Slowey, E. Bass, J. L. Chau, and S. Close (2009), Remote sensing lower thermosphere wind profiles using non-specular meteor echoes, *Geophys. Res. Lett.*, 36, L09817, doi:10.1029/2009GL037353.

Patra, A. K., T. Yokoyama, M. Yamamoto, T. Nakamura, T. Tsuda, and S. Fukao (2007), Lower E region field-aligned irregularities studied using the Equatorial Atmosphere Radar and meteor radar in Indonesia, *J. Geophys. Res.*, 112, A01301, doi:10.1029/2006JA011825.

Rees, D., A. Aruliah, T. J. Fuller-Rowell, V. B. Wickwar, and R. J. Sica (1990), Winds in the upper mesosphere at mid-latitude: First results using an imaging FPI, *Geophys. Res. Lett.*, 17, 1259–1262, doi:10.1029/GL017i009p01259.

Sugar, G., M. M. Oppenheim, E. Bass, and J. L. Chau (2010), Nonspecular meteor trail altitude distributions and durations observed by a 50 MHz high-power radar, *J. Geophys. Res.*, 115, A12334, doi:10.1029/2010JA015705.

Tsutsumi, M., D. A. Holdsworth, T. Nakamura, and I. M. Reid (1999), Meteor observations with an MF radar, *Earth Planets Space*, 24, 1591–1600.

Vincent, R. A., and I. M. Reid (1983), HF Doppler measurements of meso-spheric momentum fluxes, *J. Atmos. Sci.*, 40, 1321–1333, doi:10.1175/1520-0469(1983)040<1321:HDMOMG>2.0.CO;2.

Zhou, Q. H., Y. T. Morton, J. D. Mathews, and D. Janches (2004), Aspect sensitivity of VHF echoes from field aligned irregularities in meteor trails and thin ionization layers, *Atmos. Chem. Phys.*, 4, 685–692, doi:10.5194/acp-4-685-2004.

Y.-H. Chu, Institute of Space Science, National Central University, Chung-Li 320, Taiwan.

B. K. Dolman, ATRAD Pty Ltd., Adelaide, SA 5031, Australia.

L. Hu, G. Li, and B. Ning, Beijing National Observatory of Space Environment, Institute of Geology and Geophysics, Chinese Academy of Sciences, Beijing 100029, China. (gzlee@mail.iggcas.ac.cn)

I. M. Reid, Department of Physics and Mathematical Physics, University of Adelaide, Adelaide, SA 5005, Australia.